IEEJ TRANSACTIONS ON ELECTRICAL AND ELECTRONIC ENGINEERING

VOLUME 10, NO. 6, NOVEMBER 2015

OFFICIAL JOURNAL OF THE INSTITUTE OF ELECTRICAL ENGINEERS OF JAPAN

SCI registered

電気学会

WILEY
ISSN 1931-4973

INSTITUTE OF ELECTRICAL ENGINEERS OF JAPAN

IEEJ
TRANSACTIONS ON ELECTRICAL AND ELECTRONIC ENGINEERING
OFFICIAL JOURNAL OF THE INSTITUTE OF ELECTRICAL ENGINEERS OF JAPAN

The Institute of Electrical Engineers, Japan, Head office: Homat Horizon Bldg.8F., 6-2 Gobancho, Chiyoda-ku, Tokyo 102-0076, Japan

IEEJ

TRANSACTIONS ON ELECTRICAL AND ELECTRONIC ENGINEERING

TABLE OF CONTENTS

VOL.10, NO.6, 2015

PAPERS

Continued overleaf

IEEJ TRANSACTIONS ON ELECTRICAL AND ELECTRONIC ENGINEERING
IEEJ Trans 2015
Published online in Wiley Online Library (wileyonlinelibrary.com). DOI:10.1002/tee.22146

Paper

Adaptive B-Spline Neural Network-Based Vector Control for a Grid Side Converter in Wind Turbine-DFIG Systems

Iwan Setiawan[*,**a], Non-member
Ardyono Priyadi[*], Non-member
Hajime Miyauchi[***], Senior Member
Mauridhi Hery Purnomo[*], Non-member

This paper presents a novel control system design for the grid-side converter of doubly fed induction generator wind power generation systems. The control method proposed in this work is a vector control based on adaptive B-spline neural network by using a simple fixed-gain stabilizing control topology. The adaptive control is designed both for inner current loops and an outer DC-link voltage loop of the grid side converter control system. To guarantee the control stability, the weights updating rule for the B-spline neural network is synthesized by utilizing Lyapunov's direct method. To verify the effectiveness of the proposed control system, extensive simulations are performed using MATLAB/Simulink. Based on the simulation results, it is concluded that the proposed controller has improved performance compared to an optimum proportional integral control system. It is also relatively robust against external disturbances and variations of the control parameters. © 2015 Institute of Electrical Engineers of Japan. Published by John Wiley & Sons, Inc.

Keywords: grid side converter, adaptive B-spline neural networks, fixed-gain stabilizing control topology, Lyapunov's direct method

Received 20 October 2014; Revised 30 January 2015

1. Introduction

The rapid depletion of fossil fuels and serious environmental concerns have been encouraging the nations in the world to develop power generation systems based on renewable energy sources extensively. One of the green power generation systems that is important and has registered fast growth around the world is the doubly fed induction generator (DFIG)-based wind turbine generation system [1–4].

In a DFIG system, the stator windings of the generator are directly connected to the three-phase grid while the rotor windings are connected to the grid via back-to-back AC/DC/AC converters. From the control system point of view, these converters can be separated into two independent converters: a rotor-side converter (RSC) and a grid-side converter (GSC) [5–7]. The success of DFIG-based power generation basically depends on the control performance of these two converter control systems. However, in many papers the detailed design of those controllers is oversimplified, or even neglected [8].

Because of their ease of implementation, up to now, proportional integral (PI)-based controllers are generally utilized both for the RSC and the GSC [9]. To get the optimal response of the control system, at the design stage the control designer should know the plant model and the plant parameters accurately. To avoid these difficulties, several papers have proposed intelligent and adaptive techniques such as fuzzy logic control and system management control (SMC) [9,10].

In this paper, we focus on the controller design for the GSC in DFIG systems. However, the proposed design method basically could be applied directly to the design the control system for the RSC as well. The control method used for the converter is vector control based on adaptive B-spline neural network (BSNN) [11]. The use of BSNN as an adaptive component is based on the fact that this neural network has several advantages over other types of neural networks, such as a local learning scheme and fast learning convergence. So this neural network is more suitable for real-time control implementations.

Because the adaptive BSNN is used directly as an online controller, an appropriate control topology is a must. In this work, a simple fixed-gain stabilizing control topology is chosen as the basic structure of the controller. This control topology was proposed for the first time by Miller *et al*. In their original paper, Miller *et al*. used a cerebellum model articulation controller (CMAC) as an adaptive component for that control structure, and the adaptive component simply used the total output control as learning signals without proof of stability [12,13].

Differ from Miller's work, to guarantee the stability of the designed adaptive BSNN control system, in this work the weights updating rule is synthesized by utilizing Lyapunov's direct method. This method basically is a tool for determining the stability of dynamical systems and synthezing adaptive controllers. To show the effectiveness of the proposed controller, we compared the proposed control system performance with that of optimum PI controllers [14,15].

The remainder of this paper is organized as follows. Section 2 describes the components of the GSC model and short theories of the adaptive BSNN. The proposed control design is discussed in depth in Section 3. Next, Section 4 shows the simulation results and discusses the performance of the proposed controller. Finally, conclusions are drawn in Section 5.

[a] Correspondence to: Iwan Setiawan. E-mail: setiaone.iwan@gmail.com

[*] Department of Electrical Engineering, Institut Teknologi Sepuluh Nopember, Jalan Raya ITS, Campus ITS Sukolilo, Jawa Timur 60111, Indonesia
[**] Department of Electrical Engineering, Diponegoro University, Jl. Prof Soedarto SH, Tembalang, Semarang, Jawa Tengah 50275, Indonesia
[***] Graduate School of Science and Technology, Kumamoto University, 2-39-1Kurokami Chuo-ku, 860-0862 Kumamoto, Kumamoto, Japan

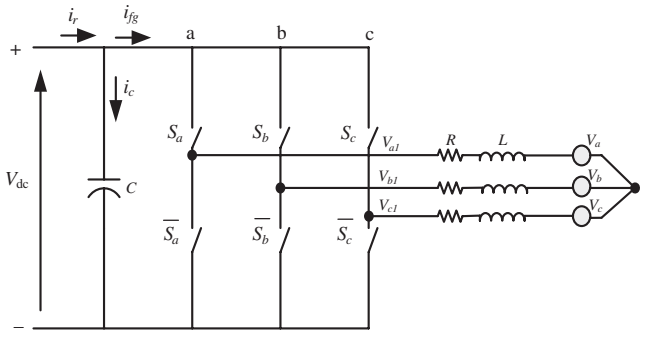

Fig. 1. Grid-side converter model

2. System Model

2.1. Control system of the GSC The major role of the GSC control system is to control the flow of the active power in both directions from the DFIG rotor windings to the three-phase electrical grid, or vice versa. The bidirectional transmission of the electrical power is accomplished indirectly by regulating the DC-link voltage of the AC/DC/AC converter, as shown in Fig. 1.

The direction of the power flow in the GSC is essentially determined by the rotational speed of the rotor. If the rotor turns faster than the synchronous speed of the generator, the DC link voltage will tend to increase. This is due to the active power flow from the rotor toward the DC link. To maintain the DC-link voltage at a certain level, the excess energy in the capacitor should be pumped by the converter to the grid; in other words, in this condition the GSC should be able to behave as an inverter.

Conversely, if the rotor turns slower than the synchronous speed of the generator, the DC link voltage will tend to decrease. This is because the electrical power flows from the DC link to the rotor. To maintain the DC-link voltage at a certain level, the GSC should be able to drain power from the grid towards the DC link capacitor; in other words, in this condition the GSC behaves as a rectifier.

For vector control design purposes, it is necessary to transform a three-phase variable model of the GSC to a rotated dq model as shown in (1) and (2).

$$v_{df} = R_f i_{df} + L_f \frac{di_{df}}{dt} + v_{dg} - \omega_s L_f i_{qf} \tag{1}$$

$$v_{qf} = R_f i_{qf} + L_f \frac{di_{qf}}{dt} + v_{qg} + \omega_s L_f i_{df} \tag{2}$$

where i_{df}, i_{qf}, v_{df}, v_{qf}, v_{dg}, v_{qg}, respectively, are currents and voltages of the inverter and the grid in the dq-axes. R_f and L_f are the parasitic resistance and the inductance of the filter, and ω_s is the synchronous speed. For this model, the active and reactive power on the grid side can be formulated, respectively, as

$$P_g = \frac{3}{2} Re\{\vec{v}_g . \vec{i}_f^*\} = \frac{3}{2}(v_{dg} i_{df} + v_{qg} i_{qf}) \tag{3}$$

$$Q_g = \frac{3}{2} Im\{\vec{v}_g . \vec{i}_f^*\} = \frac{3}{2}(v_{qg} i_{df} - v_{dg} i_{qf}) \tag{4}$$

To decouple the active and the reactive power control in (3) and (4), the rotated dq-axes frame reference should be able track the rotated grid voltage vector accurately. If the rotated dq-axes are perfectly aligned with the rotated grid voltage vector, the active and reactive power on the grid can be simplified as shown in (5) and (6), respectively.

$$P_g = \frac{3}{2}(v_{dg} i_{df}) \tag{5}$$

$$Q_g = \frac{3}{2}(-v_{dg} i_{qf}) \tag{6}$$

From (5) and (6), the active and the reactive grid power can be controled by the reguation of the d-axis and the q-axis current component of the inverter, respectively.

In the GSC control system, the reference of the d-axis current component is derived from the output of the DC link loop control. Figure 2 shows a general block diagram of the complete vector

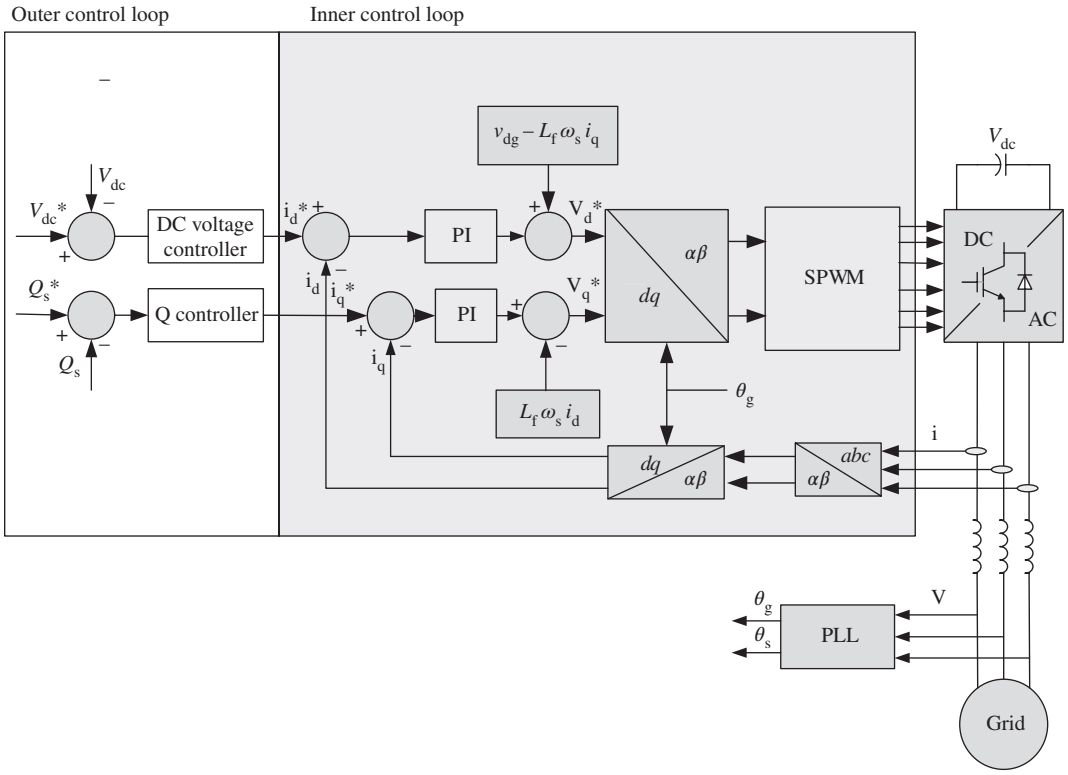

Fig. 2. General block diagram of a GSC control system

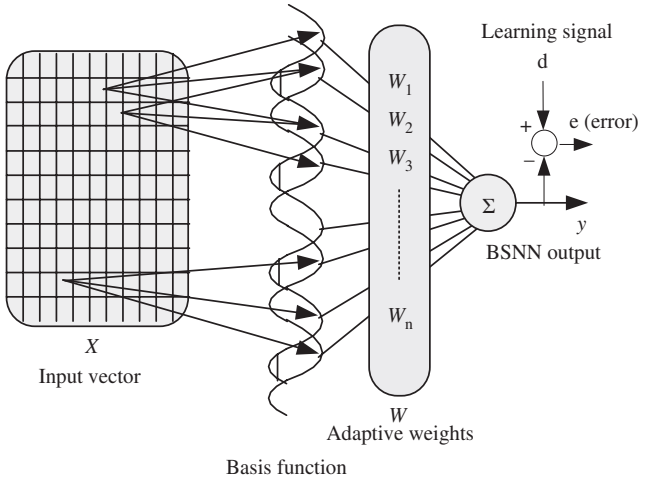

Fig. 3. Schematic diagram of the B-spline neural network

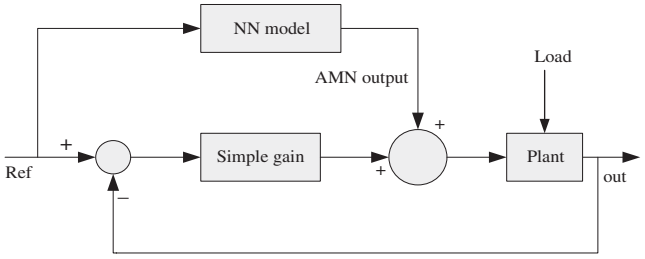

Fig. 4. Basic adaptive neural network-based control topology

control of the GSC. In that figure, the phase angle of the grid voltage is detected by the phase-locked loop (PLL) feedback control system.

For modeling purposes, the converter in the Fig. 2 can be modeled as ideal bidirectional switches. The voltage output of the converter can be represented as shown in (7).

$$\begin{bmatrix} v_{af} \\ v_{bf} \\ v_{cf} \end{bmatrix} = \frac{V_{dc}}{3} \begin{bmatrix} 2 & -1 & -1 \\ -1 & 2 & -1 \\ -1 & -1 & 2 \end{bmatrix} \begin{bmatrix} S_a \\ S_b \\ S_c \end{bmatrix} \tag{7}$$

where S_a, S_b, and S_c are signal commads to the upper side of the converter. V_{dc} is the voltage of the DC link capacitor, which depends on current flowing through the capacitor, and this can be represented as

$$V_{DC} = \frac{1}{C} \int i dt \tag{8}$$

In this case, the current through the capacitor can be found [16] as

$$i = i_{dc\_rotor} - i_{dc\_grid} \tag{9}$$

$$i_{dc\_grid} = S_a i_{ag} + S_b i_{bg} + S_c i_{cg} \tag{10}$$

2.2. BSNN and fixed-gain stabilizing control topology

In the field of artificial neural network research, BSNN can be categorized as an associative memory network (AMN), which has the local learning property.

Figure 3 shows a schematic diagram of the BSNN. From the figure, it appears that for every single input vector there are only a definite number of basic functions that are activated. Mathematically, the input–output relationship of the BSNN is represented [17,18] as

$$y(k) = \sum_{i=1}^{p} a_i(k) w_i(k) \tag{11}$$

where a(.) and $w(.)$, respectively, are the basis function output and the adaptive weights. For details of the BSNN algorithm, the readers may refer to [18].

In this work, the BSNN as an adaptive controller is implemented by using a fixed-gain stabilizing controller topology as shown in Fig. 4. There are two main controllers in this scheme: a simple ordinary feedback control loop, and an adaptive BSNN control loop.

The ordinary loop is just a simple proportional-gain feedback control loop that serves as the primary stabilizing control system, while the adaptive BSNN control loop basically is a feedforward control system that serves to increase the precision of the control system such that the overall control system can bring the output of the controlled plant to the reference. In this control structure, we can also assume that the adaptive BSNN serves as an adaptive integrator that minimizes the steady-state error of the control system.

3. The Inner Current and The Outer DC-Link Loop Control Design

3.1. The inner current loop control design In the standard differential equation form, the dynamics of the dq-axes current of the GSC system can be represented as shown in (12) and (13):

$$\frac{di_{df}}{dt} = -\frac{R_f}{L_f} i_{df} + \frac{1}{L_f} v_{df} + \frac{1}{L_f} d_{df} \tag{12}$$

$$\frac{di_{qf}}{dt} = -\frac{R_f}{L_f} i_{qf} + \frac{1}{L_f} v_{qf} + \frac{1}{L_f} d_{qf} \tag{13}$$

where d_{df} and d_{qf} are the disturbances, given by

$$d_{df} = (-v_{dg} + \omega_s L_f i_{qf}) \tag{14}$$

$$d_{qf} = (-\omega_s L_f i_{df}) \tag{15}$$

To compensate for those disturbances, we can design a simple feed-forward control to each control loop as shown in (16) and (17).

$$v_{dff} = -d_{df} \tag{16}$$

$$v_{qff} = -d_{qf} \tag{17}$$

With those compensation controls, the dynamics of the dq-axes current can be simplified as

$$\frac{di_{xf}}{dt} = -\frac{R_f}{L_f} i_{xf} + \frac{1}{L_f} v_{xf}, x = d, q \tag{18}$$

Referring to the control topology in Fig. 4, the total control output (v_{xf}) can be represented by

$$v_{xf} = u_p + u_b = K_p e + u_b \tag{19}$$

where e, and u_b, respectively, are the error and the BSNN output:

$$e = i_{xf} * - i_{xf} \tag{20}$$

$$u_b = \sigma^T W \tag{21}$$

where σ and W, respectively, are a vector of the basis functions and a vector of the adaptive weights. By substituting (19)–(21) to (18), and assuming the current reference is relatively constant, we get the dynamics of the error as

$$\dot{e} = -\left(\frac{R_f}{L_f} + \frac{1}{L_f} K_p\right) e - \frac{1}{L_f} (\sigma^T W - R_f i_{xf} *) \tag{22}$$

From (22), it is seen that the BSNN output $u_b = \sigma^T W$ mathematically does not influence the feedback loop control stability. As

long as K_p is a small positive number and u_b is nearly constant, the feedback control system will be stable. Also, based on that relation, if R_f is known accurately, the output of the BSNN can be found by using (23):

$$\sigma^T W = R_f i_{xf} * \tag{23}$$

However, in reality R_f generally is not known accurately and possibly is time-varying, so we should have a mechanism to change the output of the BSNN weights online. In this paper, we propose the utilization of the direct Lyapunov stability method to synthesize the weights updating rule for the adaptive BSNN. Choose a scalar positive definite Lyapunov function candidate as shown in (24):

$$V(e, W) = \frac{1}{2}e^2 + \frac{1}{2}(\sigma^T W - R_f i_{xf} *)^2 \tag{24}$$

For the above Lyapunov function candidate, its derivative is given by

$$\dot{V}(e, W) = e\dot{e} + (\sigma^T W - R_f i_{xf} *)\sigma^T \dot{W} \tag{25}$$

By ssubstituting (22) into (25) and with a little simplification, we get

$$\dot{V}(e, W) = -\left(\frac{R_f}{L_f} + \frac{1}{L_f}K_p\right)e^2 - (\sigma^T W - R_f i_{xf}{}^*)\frac{1}{L_f}e + (\sigma^T W - R_f i_{xf}{}^*)\sigma^T \dot{W} \tag{26}$$

Referring to the last equation, if we choose

$$\sigma^T \dot{W} = \frac{1}{L_f}e \tag{27}$$

or

$$\dot{W} = \frac{e}{(\sigma^T \sigma)L_f}.[\sigma] \tag{28}$$

then the time derivative of the Lyapunov function will have the following form:

$$\dot{V}(e, W) = -\left(\frac{R_f}{L_f} + \frac{1}{L_f}K_p\right)e^2 \tag{29}$$

From (29), we find that the derivative of the Lyapunov function would be negative as long as the error is not equal to zero. In other words, the weights updating rule represented in (28) would make the control system stable (negative definite). Further, because L_f is relatively constant, (28) can be simplified as

$$\dot{W} = \frac{\alpha e}{\sigma^T \sigma}.[\sigma] \tag{30}$$

In the discrete form, the above relation can be represented as

$$W_{K+1} = W_K + \Delta W \tag{31}$$

where

$$\Delta W = \frac{\alpha e}{\sigma^T \sigma}.[\sigma] \tag{32}$$

In this case, the range of the learning rate α is between 0 and 1. The lower the learning rate, the less the changes of the weights.

Because the variable e that appears in (32) is actually the plant output error, for a certain learning rate, large changes of the weights will primarily occur at transient states (i.e., when there is a change in the reference). Because the total control output comes from the combination of the ordinary feedback loop control and the adaptive BSNN loop control, large changes of the weights can make the plant output experience excessive overshoot in the transient state. To avoid these problems, we can minimize the value of the learing rate in (32). On the other hand, if the chosen learning rate is too small, the system response would also be slower for each transition state. In order for the control system output to keep running fast at the transient state without inducing overshoot or undershoot excessively, in this work, besides the control system output error, we also use the error derivative as a free variable for updating the BSNN weights as represented by (33).

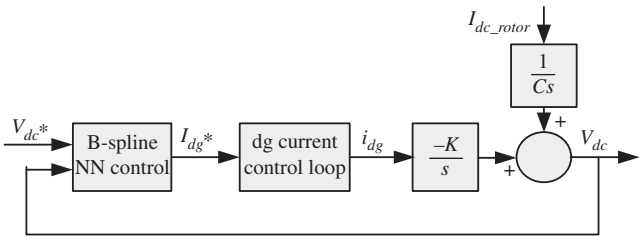

Fig. 5. Block diagram of the DC link control system

$$\Delta W = \frac{\alpha(e + K_d\dot{e})}{\sigma^T \sigma}.[\sigma] \tag{33}$$

where K_d is a small positive constant that could be chosen empirically. In this case, the effect of the $K_d\dot{e}$ term is to limit the weights changes (ΔW) when the error decreases too drastically: the greater the K_d, the lsmaller the weight changes and the more damped the output control system.

3.2. The outer DC link control loop design The main role of the outer control loop basically is to regulate DC link voltage of the capacitor. If the control system works properly, then the power generated in the RSC at the oversyncronous conditions can be pumped to the electrical grid automatically, and the active power needed in the RSC at the subsynchronous condition can be drained from electrical grid. Assuming that the converter is a lossless component and the reactive power transfer to the grid is zero, the power flow in the DC link should be equal to the active power in the GSC:

$$V_{dc} i_{dc\_grid} = \frac{3}{2}(v_{dg} i_{df}) \tag{34}$$

Using SPWM with third harmonic injection, the relation of v_{dg} can be written as

$$v_{dg} = m_a \frac{V_{dc}}{\sqrt{3}} \tag{35}$$

By substituting (35) into (34), the DC current flowing in DC link circuit can be represented by

$$i_{dc\_grid} = \frac{3}{2}\frac{m_a}{\sqrt{3}} i_{df} \tag{36}$$

So the dynamic of the capacitor voltage that is represented in (8) can be written as

$$\frac{V_{DC}}{dt} = -K_{int} i_{df} + \frac{1}{C} i_{dc\_rotor} \tag{37}$$

where

$$K_{int} = \frac{3}{2}\frac{m_a}{\sqrt{3}C}$$

From (37) it can be seen that the capacitor voltage practically can be controlled by regulating the d-axis current component. Figure 5 shows the block diagram of the DC link control system.

By using the fact that the dynamics of the inner current loop is very fast compared to the outer voltage loop control dynamics, we can neglect the former. With this assumption, (37)can be represented as

$$\frac{V_{DC}}{dt} = -K i_{df}^* + \frac{1}{C} i_{dc\_rotor} \tag{38}$$

Referring to the fixed-gain stabilizing controller topology, the d-axis current reference can be represented as

$$i_{df}^{*} = K_P e + U_b \tag{39}$$

where e and u_b, respectively, are the error and the BSNN outputs.

$$e = V_{dc} - V_{dc}^{*} \tag{40}$$

Using the fact that the reference of the DC link is constant, the error dynamics can be found:

$$\dot{e} = -KK_p e - K\left(\sigma^T W - \frac{1}{KC} i_{dc\_rotor}\right) \tag{41}$$

As with the current loop control design procedure, the derivation of the weights updating rule for the outer control loop can be explained as follows. Choose a scalar positive-definite Lyapunov function candidate as shown in (42):

$$V(e, W) = \frac{1}{2}e^2 + \frac{1}{2}\left(\sigma^T W - \frac{1}{KC} i_{dc\_rotor}\right)^2 \tag{42}$$

The time derivative of V (.) is given by

$$\dot{V}(e, W) = e\dot{e} + \left(\sigma^T W - \frac{1}{KC} i_{dc\_rotor}\right)\sigma^T \dot{W} \tag{43}$$

By substituting (41) in to the last equation, we get

$$\dot{V}(e, W) = -KK_p e^2 - \left(\sigma^T W - \frac{1}{KC} i_{dc_{rotor}}\right) Ke + \left(\sigma^T W - \frac{1}{KC} i_{dc\_rotor}\right)\sigma^T \dot{W} \tag{44}$$

If we choose

$$\sigma^T \dot{W} = Ke$$

or

$$\dot{W} = \frac{\alpha Ke}{\sigma^T \sigma}.[\sigma] \tag{45}$$

then the time derivative of the Lyapunov function would be negative as long as the error is not equal to zero:

$$\dot{V}(e, W) = -KK_p e^2 \tag{46}$$

With this explanation, the changes of the BSNN weights for the outer loop control will have the same form as that of (33).

4. Results and Discussion

To verify the performance of the adaptive BSNN-based controller, extensive simulations under MATLAB/Simulink environment have been performed. The parameters of the GSC model for the simulation are shown in Table I.

For comparison purposes, we also simulate the GSC control by using the PI control strategy. Because the inner current loop can be approximated as a first-order model, The optimum parameters for the PI control in the inner loop are derived by using the pole placement technique. The optimum parameters for the PI control in the outer DC-link voltage loop are derived by using the symmetric optimum method. Table II shows the optimal PI control parameters calculated using those methods.

4.1. Performance of the inner current loop control

To guarantee the stability of the control system, we should determine the adaptive BSNN parameters (i.e., K_p, α, and K_d) appropriately. Because the BSNN control block basically serves as an integrator, the optimal K_p parameter can be determined by using the same technique as we used to compute the optimal parameter for the PI control (In this work, the optimal K_p parameter in Table II is be used for the BSNN control). For α and K_d, although the optimal values could be determined by using heuristic optimization approaches, in this work, we chose those parameters empirically, the objective being to show the influence of the variation of the parameters on the performance of the control system (the investigation of the optimal BSNN parameter will be the subject of future work).

Table I. Plant and control parameters

Plant and control parameter	Value
R_f	0.02 Ω
L_f	0.01 H
C	1200 μF
DC link voltage	650 V
Grid voltage (rms)	220 V
Grid frequency	50 Hz
SPWM frequency	10 kHz
Time sampling	0.0001 s
BSNN order	3

Table II. Optimal PI parameters for comparison purposes

Loop	Parameter	Optimal value	Method
Inner	K_p	10	Pole placement (Closed loop time constant, $T_{in\_cl} = 0.001\,s$):
	T_i	0.5 s	$K_p = L_f/T_{in\_cl}$ $T_i = L_f/R_f$
Outer	K_p	0.56	Symmetric optimum ($a = 3$): $K_p = 1/(3K_{int}T_{in\_cl})$
	T_i	0.009 s	$Ti = 9T_{in\_cl}$

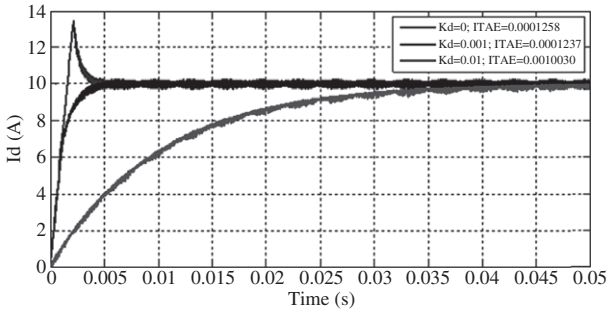

Fig. 6. Effect of the variation of the K_d parameter (for fixed $\alpha = 0.1$) on a step change response

By using the optimal proportional gain (i.e. $K_p = 10$ as shown in Table II) and a moderate learning rate (i.e., $\alpha = 0.1$), the effect of K_d on the performance of the control system can be seen clearly from Fig. 6. As we have described in the design section, the bigger the K_d value we choose, the more damped will be the output response; but on the other hand, if we choose too small a K_d (e.g., $K_d = 0$), then the output response will experience excessive overshoot. From extensive simulations, the appropriate K_d were chosen in range 0–0.001. By using K_d in this range, the output response will generate almost the same integral of time and absolute error (ITAE). Figure 7 shows the capability of BSNN control to track the reference changes by using the relatively small K_d (i.e., $K_d = 0.0005$).

From Fig. 7(a) we can see that the respone of i_{df} for the changes of the reference at the time 0, 0.06, and 0.12 s has very fast transient time. For i_{df} plotted in the Fig. 7(a), the corresponding

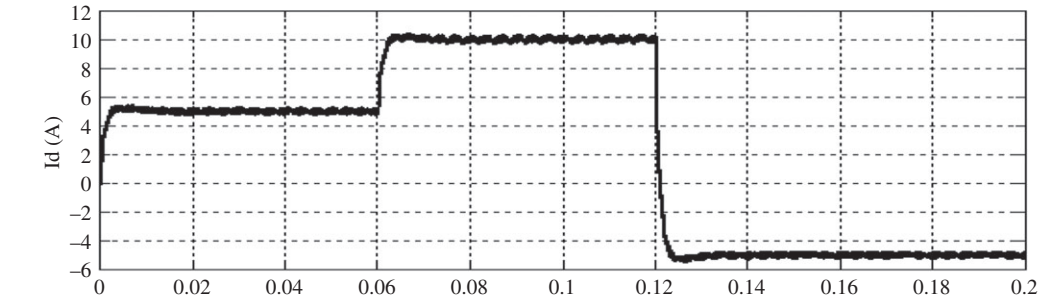

(a) *d*-axis current step changes

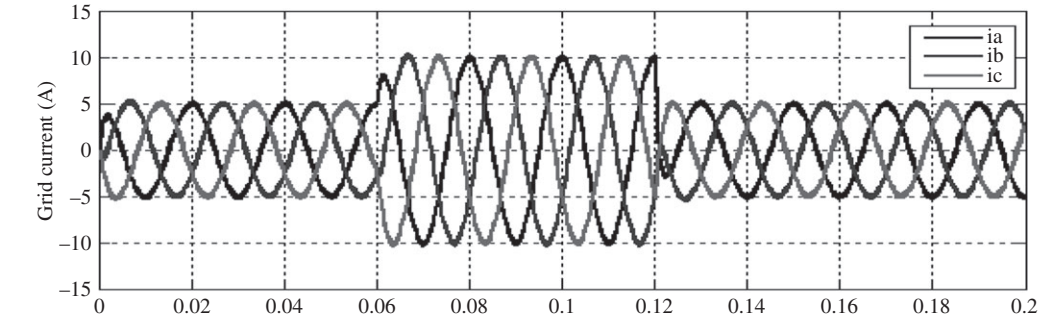

(b) Three phase current injected to grid

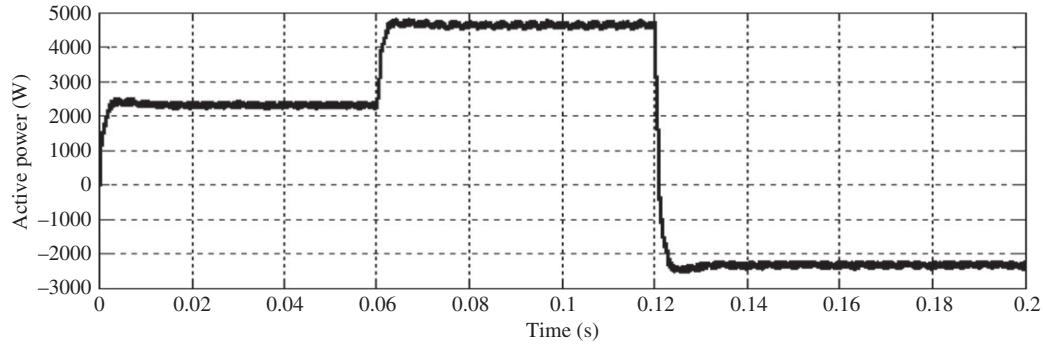

(c) Active power injected/drawn to/from grid

Fig. 7. Response of current and active power to the reference step changes of d-axis current component (reference of $i_{qf} = 0$ and $\alpha = 0.1$)

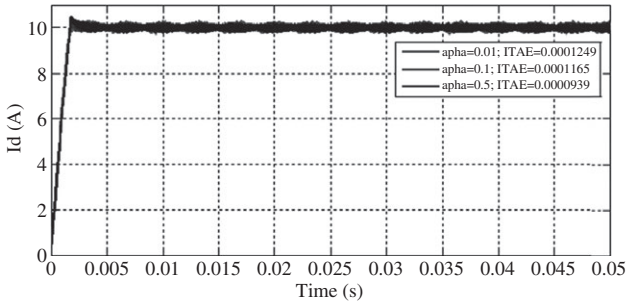

Fig. 8. Responses of the BSNN control for several values of the α parameter

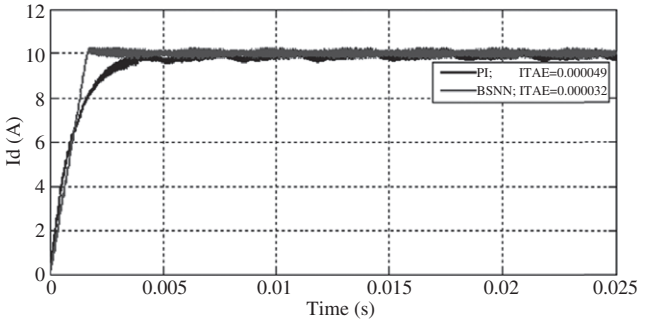

Fig. 9. Comparison of the transient response of the optimum PI control and the BSNN control system ($\alpha = 0.1$)

three-phase current and the active power at the grid side are shown, respectively, in Fig. 7(b) and (c).

From Fig. 7(b), it is seen that the maximum value of the three-phase current has the same magnitude as i_{df}, whereas the polarity of the current depends on the polarity of i_{df}: For positive polarity of i_{df} (from the time of 0 to 0.12s), the polarity of i_a, i_b, and i_c, respectively, will be the same as the polarity of v_a, v_b, and v_c. If the polarity of i_{df} is negative (after the time of 0.12 s), then the three-phase currents i_a, i_b, and i_c, respectively, will be reversed or have a different polarity than v_a, v_b, and v_c (however, for the clarity of the figure, the three-phase grid voltage waveform is not plotted in that figure). From Fig. 7(c) we can see that the polarity of the active power will be the same as the polarity of i_{df}, which is plotted in Fig. 7(a).

For an arbitrarily small K_d, the effect of the learning rate variation can be seen from Fig. 8. The interesting result derived from the figure is that the control performance of the inner current loop is robust to the learning rate variation; a significant difference in the learning rate does not influence the transient response of the control output.

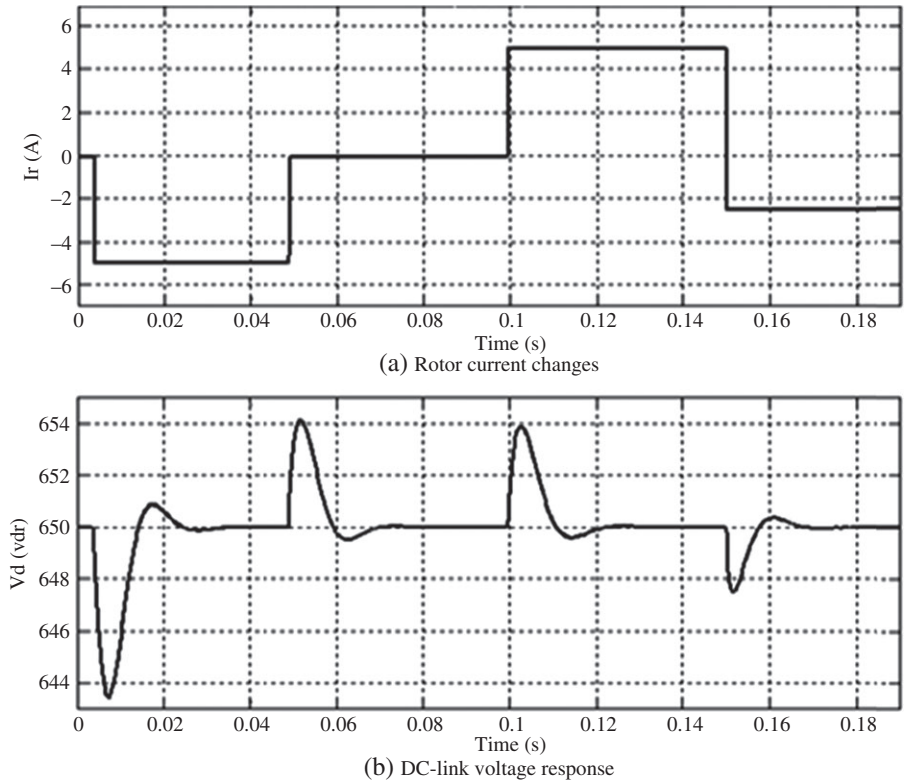

(a) Rotor current changes

(b) DC-link voltage response

Fig. 10. Response of the DC-link voltage to the DC rotor current step changes ($\alpha = 0.00005$)

The superiority of the BSNN control system compared to the PI control can be seen from Fig. 9. Although both the responses have nearly the same time constant (0.001 s), from the figure we can see that the settling time for BSNN response is faster than that of the PI control.

4.2. Performance of the outer DC-link loop control

Generally, the design procedure for the outer DC-link voltage loop control is the same as that of the inner current loop control. In this case, we should choose the appropriate parameters of the BSNN control system so that the performance of the control system is acceptable. As with the inner loop control, the K_d that is used in the outer loop control is fixed, that is 0.0005, whereas the K_p that is used is the same as the optimal K_p parameter shown in Table II. In this section, we will investigate deeply the effect of the variation of the α and also compare the results with those of PI control.

The main objective of the outer DC-link voltage control is to maintain the capacitor voltage level at the prescribed constant value (i.e., 650 V) regardless of changes to both the magnitude and the direction of the DC rotor current. Figure 10 shows the response of the BSNN control system (with α = 0.00005) to the change of the DC rotor current that serves as disturbance. From the figure, we can see that the control system is very stable with regard to the disturbances and has a relatively fast settling time.

Compared to the inner loop control, the α that is used for the outer loop control should be small. If we set α too large, the control system will experience oscillations or even become unstable. Figure 11 shows the response of the BSNN control for several values of α. From the figure we can conclude that for the outer loop control, the BSNN control system is very sensitive to the variation of the learning rate parameter (it does not happen in the case of the inner loop control). This is a direct consequence of the weights updating rule derivation in

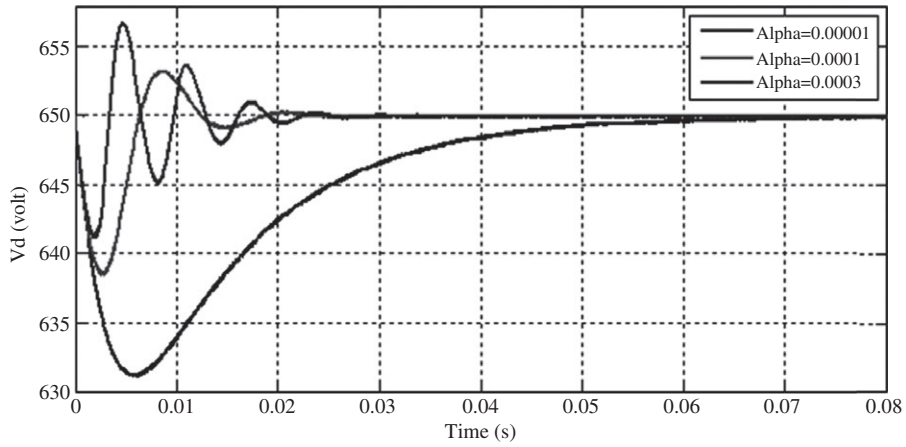

Fig. 11. Response of the DC-link voltage to the DC rotor current step changes for several values of the α parameter

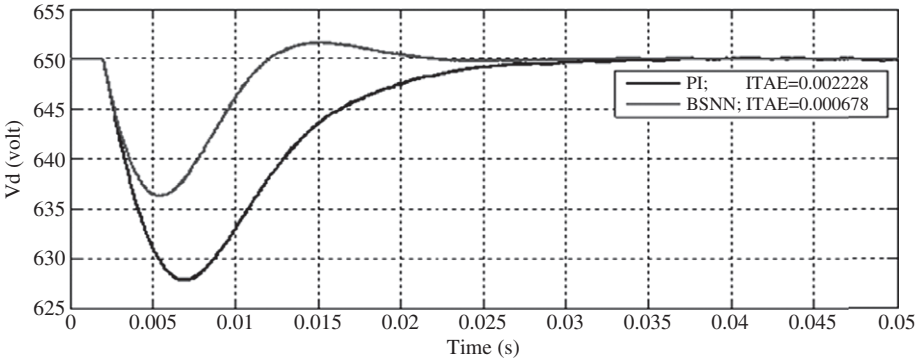

Fig. 12. Comparison of the DC-link voltage response of the PI and the BSNN controller to the DC rotor current step change

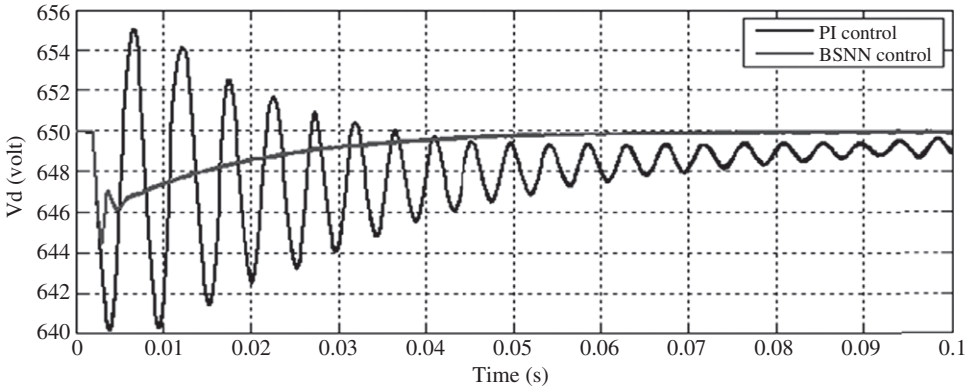

Fig. 13. Comparison of the DC-link voltage responses of the PI control and the BSNN control system by using a nonoptimal value of K_p (i.e. $K_p = 2.8$)

Table III. Performance of the PI and the BSNN control System from Fig. 12.

Control strategy	Undershoot (%)	Settling time (s)	ITAE
The PI control (both the inner and the outer loop)	3.3	0.03	0.002228
BSNN control (both the inner and the outer loop)	2	0.02	0.000678

the BSNN design (Section 3.2), which is in this case, for the simplification of the derivation of the weights updating rule, we have neglected in the dynamic model of the inner current loop control. In order to make the learning process and control system run stably, the weight changes of the BSNN should be done more gradually than the inner loop control (i.e., by using the lower α).

Using the relatively small learning rate (i.e., α = 0.00005), the superiority of the BSNN control system over the PI control can be seen from Fig. 12. From the figure we can see that for the DC rotor current step changes (i.e., 10 A), the response of the BSNN control system is better than the PI control response. Table III lists several performance indexes derived from those responses.

Although the outer loop control is not very robust compared to the inner one, the robustness of BSNN control to the variation of the K_p parameter is far better compared to the PI control, as we can see from Fig. 13. From the figure we can see that for a nonoptimal K_p value, the response of the BSNN control system to the DC rotor current step change (i.e., 10 A) is still stable compared to the response of the PI control.

5. Conclusions

In this paper, an adaptive BSNN control system both for tracking the current reference in the inner loops and regulating the DC link voltage in the outer loop of the GSC system was proposed. From the simulation results we could see that the performance of the inner current loop control was almost insensitive to the learning rate variation. For the wide span of the chosen learning rate, the performance of the BSNN control system was superior to that of the optimal PI control system, whereas because of the simplification of the outer loop model, the performance of the outer DC-link loop control is very sensitive to the variation of the learning rate. However, by using the appropriate small learning rate, we have seen from the simulations that the dynamic responses and the performance index of the BSNN control system are far better than those of the PI control that is tuned by the popular symmetrical optimum method.

In future work, we will investigate the optimal parameters of the BSNN control system by using heuristic optimization approaches.

Acknowledgments

The first author wishes togratefully acknowledge the full financial support received from the Indonesian Directorate General of Higher Education both for pursuing the doctoral program at ITS, Indonesia, and carrying out research at the Graduate School of Science and Technology, Kumamoto University, Japan.

References

(1) Hansen AD, Hansen LH. Market penetration of different wind turbine concepts over the years. *2007 European Wind Energy Conference and Exhibition*, 2007.

(2) Li H, Chen Z. Overview of different wind generator systems and their comparisons. *IET Renewable Power Generation* 2008; **2(2)**:123–138.
(3) Anita BBR. Modelling, simulation and analysis of doubly fed induction generator for wind turbines. *Journal of Electrical Engineering* 2009; **60(2)**:79–85.
(4) Pena R, Clare JC, Asher GM. Doubly fed induction generator using back-to-back PWM converters and its application to variable-speed wind-energy generation. *IEE Proceedings-Electric Power Applications* 1996; **143(3)**:231–241.
(5) Tapia A, Tapia G, Ostolaza JX, Sáenz JR. Modeling and control of a wind turbine driven doubly fed induction generator. *IEEE Transactions on Energy Conversion* 2003; **18(2)**:194–204.
(6) Chowdhury BH, Chellapilla S. Double-fed induction generator control for variable speed wind power generation. *Electric Power Systems Research* 2006; **76(9)**:786–800.
(7) Muller S, Deicke M, De Doncker RW. Doubly fed induction generator systems for wind turbines. *IEEE Industry Applications Magazine* 2002; **8(3)**:26–33.
(8) Nagaria D, Pillai N, Gupta HO. Particle swarm optimazitation approach for controller design in WECS equipped with DFIG. *Journal of Electrical Systems* 2010; **6(2)**:1–17.
(9) Mishra S, Mishra Y, Li F, Dong ZY. TS-fuzzy controlled DFIG based wind energy conversion systems. *Power & Energy Society General Meeting, 2009. PES'09*. IEEE, 2009; 1–7.
(10) Bekakra Y, Ben Attous Djilani. Speed and flux control for DFOC of doubly fed induction machine using sliding mode controller. *Acta Electrotechnica et Informatica* 2010; **10(4)**:75–81.
(11) Setiawan I, Priyadi A, Purnomo MH. Controlling of non-minimum phase micro hydro power plant based on adaptive B-Spline neural network. *Information Technology and Electrical Engineering (ICITEEE), 2013 International Conference on*, 2013; 460–464.
(12) Miller WT, Glanz FH, Kraft LG. Application of a general learning algorithm to the control of robotic manipulators. *International Journal of Robotics Research* 1987; **6(2)**:84–98.
(13) Chen F-C, Chang C-H. Practical stability issues in CMAC neural network control systems. *IEEE Transactions on Control Systems Technology* 1996; **4(1)**:86–91.
(14) Preitl S, Precup R-E. An extension of tuning relations after symmetrical optimum method for PI and PID controllers. *Automatica* 1999; **35(10)**:1731–1736.
(15) Bajracharya C, Molinas M, Suul JA, Undeland TM. Understanding of tuning techniques of converter controllers for VSC-HVDC. *Nordic Workshop on Power and Industrial Electronics (NORPIE/2008)*, Espoo, Finland. Helsinki University of Technology; 2008.
(16) Abad G, Lopez J, Rodrıguez M, Marroyo L, Iwanski G. *Doubly Fed Induction Machine: Modeling and Control for Wind Energy Generation*, vol. **86.** Hoboken: John Wiley & Sons, Inc.; 2011.
(17) Cheng KWE, Wang HY, Sutanto D. Adaptive B-spline network control for three-phase PWM AC-DC voltage source converter. *International Conference on Power Electronics and Drive Systems*, Hongkong, 1999; 467–472.
(18) Brown M, Harris CJ. *Neurofuzzy Adaptive Modelling and Control*. Prentice Hall (UK): Hertfordshire; 1994.

Iwan Setiawan (Non-member) received the B.E. and M.E. degrees from Gadjah Mada University, Indonesia, in 1998 and 2003, respectively. Currently he is pursuing the Ph.D. degree at the Department of Electrical Engineering, Institut Teknologi Sepuluh Nopember, Indonesia. Since 2000, he has been a Lecturer with Diponegoro University, Indonesia. His research interests include power systems control.

Ardyono Priyadi (Non-member) received the B.E. degree from the Institut Teknologi Sepuluh Nopember (ITSN), Indonesia, in 1997, and the M.S. and Ph.D. degrees from Hiroshima University, Japan, in 2008 and 2011, respectively. He is currently a Lecturer with ITSN. His research interests include power systems and their stability.

Hajime Miyauchi (Senior member) received the B.S., M.S., and Ph.D. degrees from Kyoto University, Japan, in 1981, 1983, and 1991, respectively. He worked with Kyoto University from 1985 to 1993. Since 1993, he has been with Kumamoto University, Kumamoto, Japan, and is currently an Associate Professor. His research interests include power system control and power system economics.

M. Hery Purnomo (Non-member) received the B.E. degree from the Institut Teknologi Sepuluh Nopember (ITSN), Indonesia, in 1985, and the M.S. and Ph.D. degrees from Osaka City University, Japan, in 1995 and 1998, respectively. He is currently a Professor with ITSN. His research interests include power systems and intelligent systems.